Electronic Supplementary Material (ESI) for Soft Matter.

Polar order, shear banding, and clustering in confined active matter: Supplementary Information

Daniel Canavello, Rubens H. Damascena, Leonardo R. E. Cabral, and Clécio C. de Souza Silva

February 2, 2024

Contents

1 Calculation details of the deterministic steady-state solutions of close-packed clusters section **1**
1.1 Polarized phase 3
1.2 Vortex phase 3

2 Supplementary Figures **6**
2.1 Effect of translational noise D_t 6
2.2 Phase boundaries for different N 6

3 Supplementary Videos **8**

1 Calculation details of the deterministic steady-state solutions of close-packed clusters section

Here we present in more detail the analytical results regarding the motion of the system in the absence of noise. We start with the equations of motion of the system:

$$\dot{\boldsymbol{r}}_k + \boldsymbol{r}_k - \sum_{\substack{l=1 \\ l\neq k}}^{N} \boldsymbol{f}_{kl} = \boldsymbol{n}_k, \tag{1}$$

$$\dot{\theta}_k = \beta(\boldsymbol{n}_k \times \dot{\boldsymbol{r}}_k)\cdot\hat{z} = -\beta\left[\boldsymbol{n}_k \times \left(\boldsymbol{r}_k - \sum_{\substack{l=1 \\ l\neq k}}^{N} \boldsymbol{f}_{kl}\right)\right]\cdot\hat{z}, \tag{2}$$

for parabolic confinement and arbitrary pairwise inter-particle forces given by:

$$\boldsymbol{f}_{kl} = f(r_{kl})\frac{\boldsymbol{r}_{kl}}{r_{kl}}, \qquad \text{for } k,\, l = 1,\, 2,\, \ldots N, \tag{3}$$

are the particles indexes, $\boldsymbol{r}_k = (r_k\cos\phi_k,\, r_k\sin\phi_k)$, $\boldsymbol{n}_k = (\cos\theta_k,\, \sin\theta_k)$, $\boldsymbol{r}_{kl} = \boldsymbol{r}_k - \boldsymbol{r}_l$, and $r_{kl} = |\boldsymbol{r}_k - \boldsymbol{r}_l|$.

Now, let us investigate a general rigid body motion of the system. In this case, it is well known that the system motion consists of a translation plus a rotation of the entire system. Therefore, the position of the k^{th} particle of the system can be described by

$$\boldsymbol{r}_k = \boldsymbol{R} + \mathsf{S}\left(\phi\right)\boldsymbol{s}_k, \tag{4}$$

where $\boldsymbol{R} = \sum_{k=1}^{N} \boldsymbol{r}_k/N$ is the position of the system centroid,

$$\mathsf{S}\left(\phi\right) = \begin{pmatrix} \cos\phi & -\sin\phi \\ \sin\phi & \cos\phi \end{pmatrix}, \tag{5}$$

is the rotation matrix, ϕ is a rotation angle in a frame whose origin is at the centroid position, and $\boldsymbol{s}_k$ is the particle position in the moving frame. Substituting this equation in Eq. (1) we obtain

$$\dot{\boldsymbol{R}} + \boldsymbol{R} + \mathsf{S}(\phi)\left[\dot{\boldsymbol{s}}_k + \omega\hat{z}\times\boldsymbol{s}_k - \sum_{\substack{l=1\\ l\neq k}}^{N} \frac{f(s_{kl})}{s_{kl}}\boldsymbol{s}_{kl}\right] = \boldsymbol{n}_k, \tag{6}$$

where $\omega = \dfrac{d\phi}{dt}$, $\boldsymbol{s}_{kl} = \boldsymbol{s}_k - \boldsymbol{s}_l$, and $s_{kl} = |\boldsymbol{s}_k - \boldsymbol{s}_l|$. By summing the contributions of all particles to Eq. (6), the internal forces cancel out and we find

$$\dot{\boldsymbol{R}} + \boldsymbol{R} = \frac{1}{N}\sum_{k=1}^{N}\boldsymbol{n}_k = \langle\boldsymbol{n}\rangle\,. \tag{7}$$

As a consequence the centroid motion is governed by the average of the orientation forces of the system. Substituting back this equation in Eqs. (6) and (2) results in

$$\dot{\boldsymbol{s}}_k + \omega\hat{z}\times\boldsymbol{s}_k - \sum_{\substack{l=1\\ l\neq k}}^{N} \frac{f(s_{kl})}{s_{kl}}\boldsymbol{s}_{kl} = \mathsf{S}(-\phi)\left(\boldsymbol{n}_k - \langle\boldsymbol{n}\rangle\right), \tag{8}$$

$$\dot{\theta}_k = \beta\left[\left(\boldsymbol{n}_k\times\dot{\boldsymbol{R}}\right)\cdot\hat{z} + \left(\boldsymbol{\eta}_k\times\dot{\boldsymbol{s}}_k\right)\cdot\hat{z} + \omega\left(\boldsymbol{\eta}_k\cdot\boldsymbol{s}_k\right)\right]. \tag{9}$$

For $\dot{\boldsymbol{s}}_k = 0$ in the moving frame, the first equation is time independent if either (i) $\boldsymbol{n}_k = \langle\boldsymbol{n}\rangle$ for all particles or (ii) $\boldsymbol{\eta}_k = \mathsf{S}(-\phi)\boldsymbol{n}_k$ is time independent (all orientations rotate at the same angular velocity ω together with the whole configuration). In the former case, all the particles have the same orientation angle, that is $\theta_i = \theta_{\text{c}}$ for $i = 1, 2, \ldots N$, while in the latter the time derivative of the particles orientations are the same, i.e., $\dot{\theta}_k = \dot{\theta}_l = \omega$ for any pair of particles in the system rotating as a rigid body with angular velocity ω. Hence, any of these conditions are sufficient to warrant a rigid body motion (with no deformations) of the system.

The two particular cases above result in Eq. (9) to be rewritten as:

- For $\boldsymbol{n}_k = \langle\boldsymbol{n}\rangle = \boldsymbol{n}_{\text{c}}$ (which is equivalent to $\theta_i = \theta_{\text{c}}$) yields

$$\left(\boldsymbol{n}_{\text{c}}\times\dot{\boldsymbol{R}}\right)\cdot\hat{z} + \omega\boldsymbol{\eta}_{\text{c}}\cdot\boldsymbol{s}_k = \beta^{-1}\dot{\theta}_{\text{c}}; \tag{10}$$

- For $\dot{\theta}_k = \dot{\theta}_l = \omega$, we have:

$$\left(\boldsymbol{n}_k\times\dot{\boldsymbol{R}}\right)\cdot\hat{z} + \omega\left(\boldsymbol{\eta}_k\cdot\boldsymbol{s}_k - \beta^{-1}\right) = 0. \tag{11}$$

Therefore, for those conditions above if both the centroid motion and the rigid body rotation are present, they are intertwined in a way given by either Eq (10) or Eq. (11).

In the following sections we analyse two particular cases of interest related to the above conditions associated with rigid body motion.

1.1 Polarized phase

We denote the case $\boldsymbol{n}_k = \langle \boldsymbol{n} \rangle = \boldsymbol{n}_\mathrm{c}$ (i.e., $\theta_k = \theta_\mathrm{c}$ for all k) for all particles the *polarized state*. Let us consider one particular case in which $\omega = 0$ (i.e., the cluster does not rotate around the centroid position, $\boldsymbol{R}$). In this case, the system behaves as 'one particle' and Eq.(10) becomes

$$-\dot{R}\sin\chi_\mathrm{c} + R\dot{\varphi}\cos\chi_\mathrm{c} = \beta^{-1}\dot{\theta}_\mathrm{c}, \tag{12}$$

where $\chi_\mathrm{c} = \theta_\mathrm{c} - \varphi$ is the tilt angle and φ is the angle $\boldsymbol{R}$ makes with the horizontal axis. Meanwhile, Eq. (7) projected along and orthogonally to $\boldsymbol{R}$ gives,

$$\dot{R} + R = \cos\chi_\mathrm{c}, \tag{13}$$

$$R\,\dot{\varphi} = \sin\chi_\mathrm{c}. \tag{14}$$

Substituting these equations in Eq. (12), we obtain

$$R^2\dot{\varphi} = \beta^{-1}\dot{\theta}_\mathrm{c}. \tag{15}$$

This equation also shows that the areolar speed covered by the centroid is equal to the time derivative of the its orientation, θ_c, divided by β. This is a particular case of a more general result for active particles in elliptic harmonic confinement.[2]

The above equations are the same as the ones for one active particle in a harmonic circular confinement. Therefore, for $\beta > 1$ a time independent periodic solution is given by $\dot{R} = 0$ and $\dot{\varphi} = \dot{\theta}_\mathrm{c}$, that is the centroid performs a periodic circular motion with angular velocity, $\Omega = \dfrac{d\varphi}{dt}$. For such a case, we have

$$R = \beta^{-1/2}, \tag{16}$$

$$\Omega = \pm\sqrt{\beta - 1}, \tag{17}$$

$$\chi_\mathrm{c} = \theta_\mathrm{c} - \varphi = \arccos\left(\beta^{-1/2}\right) \quad \Rightarrow \quad \theta_\mathrm{c} = \arccos\left(\beta^{-1/2}\right) \pm \sqrt{\beta - 1}t + \theta_\mathrm{c}\,(0)\,. \tag{18}$$

1.2 Vortex phase

Consider the case in which $\dot{\theta}_k = \omega$ for all the particles and assume that the particles rotate around the origin (that is $\boldsymbol{R} = 0$ and $\boldsymbol{r}_k = \boldsymbol{s}_k$). In this case, Eq. (7) tell us that $\langle \boldsymbol{n} \rangle = 0$. Now, let us compute the angular velocity for this situation of rigid body motion. By taking the vector product between $\boldsymbol{r}_k$ and Eq. (1) and summing over the contributions of all the partilces, internal torques cancel out we find

$$\sum_k s_k^2\dot{\phi}_k = \omega\sum_k s_k^2 = \sum_k s_k\sin\chi_k, \tag{19}$$

where $\chi_k = \theta_k - \phi_k$. From Eq. (11) we have $\boldsymbol{\eta}_k \cdot \boldsymbol{s}_k = s_k \cos\chi_k = 1/\beta$. Therefore,

$$\omega = \frac{\displaystyle\sum_k \sqrt{s_k^2 - \frac{1}{\beta^2}}}{\displaystyle\sum_k s_k^2}. \tag{20}$$

This result shows us that a strict rigid body motion is possible in the vortex phase only for particles at $r > 1/\beta$.

Now let us relax the condition $\dot{\theta}_k = \omega$, which means the system is not in strict rigid body motion, while still assuming that the particles rotate around the origin with approximate fixed radial positions (i.e., $\boldsymbol{r}_k = \boldsymbol{s}_k$ with $\dot{s}_k \approx 0$) and angular velocity $\dot{\phi}_k \approx \omega$. Thus, Eq. (9) becomes,

$$\dot{\chi}_k = (\beta s_k \cos\chi_k - 1)\,\omega, \tag{21}$$

whose solution is given by, [3]

$$-\omega\, t = \int_{\chi_k(0)}^{\chi_k(t)} \frac{d\chi}{1 - \beta s_k \cos\chi} = \frac{[G(t) - G(0)]}{\sqrt{|\beta^2 s_k^2 - 1|}} \tag{22}$$

where $\chi_k(0)$ is the value of χ_k at some initial time $t = 0$ and,

$$G(t) = \begin{cases} 2\,\arctan\left[\dfrac{(1+\beta s_k)\tan(\chi/2)}{\sqrt{|\beta^2 s_k^2 - 1|}}\right], & \text{for } \beta s_k < 1, \\ \ln\left[\dfrac{\sqrt{|\beta^2 s_k^2 - 1|} - (1+\beta s_k)\tan(\chi/2)}{\sqrt{|\beta^2 s_k^2 - 1|} + (1+\beta s_k)\tan(\chi/2)}\right], & \text{for } \beta s_k > 1. \end{cases} \tag{23}$$

The above solution gives rise to two distinct time dependences of χ_k. For $s_k > 1/\beta$ there is a monotonic dependence of χ_k on time,

$$\chi_k = 2\arctan\left[\left(\frac{C_+ + C_- e^{-t/\tau_\omega}}{C_+ - C_- e^{-t/\tau_\omega}}\right)\sqrt{\frac{\beta s_k - 1}{\beta s_k + 1}}\right], \tag{24}$$

where $C_\pm = \tan\left(\chi_k(0)/2\right) \pm \sqrt{(\beta s_k - 1)\,/\,(\beta s_k + 1)}$ and $\tau_\omega = 1/\omega\sqrt{\beta^2 s_k^2 - 1}$. In this case, for $t \gg \tau_\omega$ we have the asymptotic value $\chi_k = 2\arctan\sqrt{(\beta s_k - 1)\,/\,(\beta s_k + 1)}$, which gives $\cos\chi_k = 1/\beta s_k$. This is exactly the result expected by assuming $\omega = \dot{\theta}_k$.

On the other hand, χ_k has oscillatory response for $r_k < 1/\beta$, given by

$$\chi_k = -2\arctan\left[\sqrt{\frac{1-\beta s_k}{1+\beta s_k}}\tan\left(\sqrt{1-\beta^2 s_k^2}\frac{\omega t}{2} - C_0\right)\right], \tag{25}$$

where $C_0 = \arctan\left[\sqrt{(1-\beta s_k)\,/\,(1+\beta s_k)}\tan\left(\chi_k(0)/2\right)\right]$.

These above expressions for χ_k allow us to obtain the time averages of $\boldsymbol{n}_k \cdot \boldsymbol{r}_k = s_k\cos\chi$ and $(\boldsymbol{r}_k \times \boldsymbol{n}_k)\cdot\hat{z} = s_k \sin\chi$. For that we compute the asymptotic limit of $\cos\chi_k$ and $\sin\chi_k$ for $r_k = s_k > 1/\beta$ and their time averages for $r_k = s_k < 1/\beta$. As already mentioned, for $s_k > 1/\beta$ and $t \gg 1/\omega\sqrt{\beta^2 s_k^2 - 1}$, we have $\cos\chi_k = 1/\beta s_k$, which gives

$$\boldsymbol{n}_k \cdot \boldsymbol{r}_k = s_k\cos\chi_k = \frac{1}{\beta} \qquad \text{and} \qquad (\boldsymbol{r}_k \times \boldsymbol{n}_k)\cdot\hat{z} = s_k\sin\chi_k = \sqrt{s_k^2 - \frac{1}{\beta^2}}. \tag{26}$$

For $s_k < 1/\beta$, after some straightforward calculation Eq. (25) gives

$$\sin\chi_k = -\frac{\sqrt{1-\beta^2 s_k^2}\,\sin\left(\sqrt{1-\beta^2 s_k^2}\,\omega t - 2C_0\right)}{1+\beta s_k \cos\left(\sqrt{1-\beta^2 s_k^2}\,\omega t - 2C_0\right)}, \tag{27}$$

$$\cos\chi_k = \frac{\beta s_k + \cos\left(\sqrt{1-\beta^2 s_k^2}\,\omega t - 2C_0\right)}{1+\beta s_k \cos\left(\sqrt{1-\beta^2 s_k^2}\,\omega t - 2C_0\right)}. \tag{28}$$

The time average of $\sin\chi_k$ over one period of time $T = 2\pi/\omega\sqrt{1-\beta^2 s_k^2}$ is zero since it is an odd function. On the other hand, the time average of $\cos\chi_k$ is nonzero and can be computed by using standard table of integrals [4]. Therefore,

$$\langle\sin\chi_k\rangle_T = 0 \qquad \text{and} \qquad \langle\cos\chi_k\rangle_T = \frac{1-\sqrt{1-\beta^2 s_k^2}}{\beta s_k}. \tag{29}$$

Consequently, for $s_k < 1/\beta$,

$$\langle \boldsymbol{n}_k \cdot \boldsymbol{r}_k\rangle_T = \frac{1-\sqrt{1-\beta^2 s_k^2}}{\beta} \qquad \text{and} \qquad \langle(\boldsymbol{r}_k \times \boldsymbol{n}_k)\cdot\hat{z}\rangle_T = 0. \tag{30}$$

Now, let us calculate the average angular velocity taking into account the above results. Again, by taking the vector product between $\boldsymbol{r}_k$ and Eq. (1), summing over the contributions of all the particles, and canceling out the internal torques, we find

$$\sum_k s_k^2 \dot{\phi}_k = \sum_k s_k \sin\chi_k. \tag{31}$$

Here, we use $\dot{\phi}_k \approx \omega$ and take the time average of this equation. Since $\langle(\boldsymbol{r}_k \times \boldsymbol{n}_k)\cdot\hat{z}\rangle_T = s_k\langle\sin\chi_k\rangle_T = 0$ for $r_k = s_k < 1/\beta$, Eq. (31) results in

$$\langle\omega\rangle_T = \frac{{\sum_k}' s_k \langle\sin\chi_k\rangle_T}{\sum_k s_k^2} = \frac{{\sum_k}' \sqrt{s_k^2 - \dfrac{1}{\beta^2}}}{\sum_k s_k^2}, \tag{32}$$

where ${\sum_k}'$ means sum over only the particles outside of $r = 1/\beta$, while $\sum_k$ is the sum over all the particles. This expression is similar (but not equal) to Eq. (20).

Finally, we return to Eq. (21) and take its time average. It furnishes the time average of the particles orientation angle,

$$\left\langle\dot{\theta}_k\right\rangle_T = \beta s_k \langle\cos\chi_k\rangle_T \langle\omega\rangle_T = \begin{cases} \langle\omega\rangle_T, & \text{for } s_k > \beta^{-1} \\ \left[1-\sqrt{1-\beta^2 s_k^2}\right]\langle\omega\rangle_T, & \text{for } s_k < \beta^{-1} \end{cases} \tag{33}$$

These obtained time dependencies of χ_k show that, although for $s_k > 1/\beta$ the conditions for a strict rigid body motion can be realized, that is not the case for particles inside $s < 1/\beta$. This conclusion can be seen by noticing that a time dependent χ_k implies in a time dependence of $\boldsymbol{n}_k$, which also implies that both $\dot{r}_k$ and $\dot{\phi}_k$ in Eq. (1) do depend on time. Therefore, the above results for the vortex phase are to be taken as an approximate model for the dynamics of particles moving together with the same angular velocities and with small variations of their radial distances to the origin.

2 Supplementary Figures

2.1 Effect of translational noise D_t

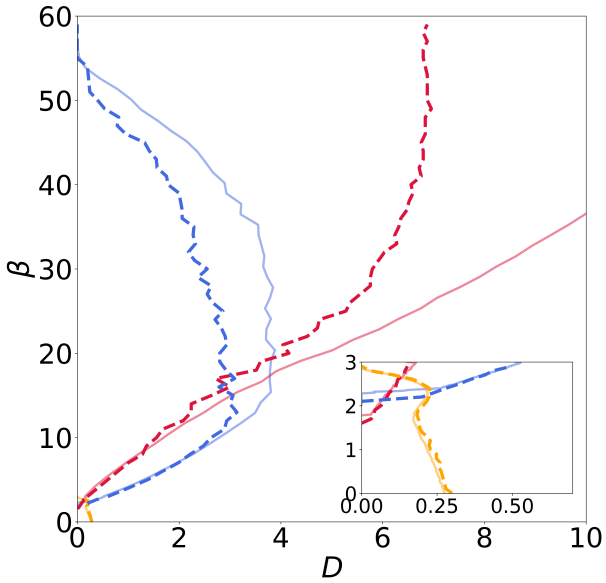

Figure 1: 0.5 contour levels of the averaged total (red), azimuthal (blue), and radial (orange) order parameters. The solid lines represent the $D_t = 0$ case considered in the main text, that is, the same as in Fig. 2. The dashed lines represent the case where translational noise $D_t = \sigma^2 D/3$ is added.

In this analysis, we explore a scenario where thermal noise, rather than the self-propulsion mechanism, serves as the primary source of fluctuations. The translational (D_t) and rotational (D) diffusion constants in this case are related by $D_t = \sigma^2 D/3$. Since for most cases of interest (our work included) particle size is small compared to other relevant length scales, D_t is typically small compared to D. On the other hand, the proportionality between both diffusion constants in the thermal noise case warrants that increasing D increases the importance of the translational noise. As illustrated in the figure, translational noise notably influences phase boundaries, particularly for larger D, with more drastic changes observed in the high β region of the phase diagram. Conversely, for $D \lesssim 1$, the phase boundaries remain essentially unchanged, whether or not D_t is present. This indicates that translational noise has a negligible effect on the radially polarized and shear-banded vortex phases. Despite alterations in phase boundaries, all phases maintain the same qualitative features observed in the case of active noise, and no new phases were detected.

2.2 Phase boundaries for different N

In Fig 2 we observe that systems with different N do not respond to noise in the same way, even when the filling fraction is made the same for all N. This difference is more pronounced in the noise-induced decay of the UV towards the FM phase. Here we set up a possible scenario that might explain this. In order to achieve the FM phase, particles need to adjust not only their local moments but also the position of the centroid, which must climb all the way up to the orbital position of the FM phase. Increasing N at a

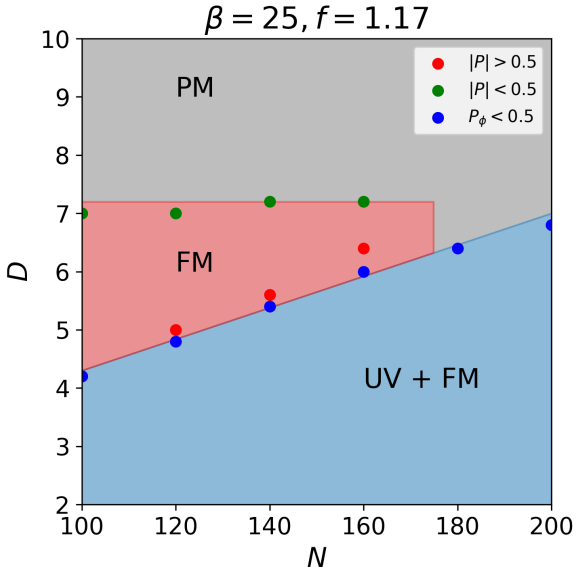

Figure 2: Noise-induced transitions for a system starting in the UV state at $D = 0$ for different values of N at fixed $f = 1.17$ (same filling fraction of the system with $N = 93$ and $\sigma = 0.2$) and $\beta = 25$. The study is performed by sweeping D from zero up to 10 and then back to 0 as in Fig. 4(a) of the main text. To keep constant f for different N we change σ using Eq. 4. The blue symbols correspond to the threshold values of D in the upward branch when $\langle\langle P_\phi \rangle\rangle < 0.5$, while the red and green symbols correspond to the threshold values of D where $\langle\langle |\boldsymbol{P}| \rangle\rangle$ increases above 0.5 and then dips below 0.5, respectively. Color shades are just guides to the eye to better identify the phases.

given value of D leads to a more effective cancellation of the Langevin kicks, thus reducing fluctuations of the centroid. Therefore, a larger value of D is needed to promote the UV-FM transition. In contrast, the FM-PM transition is dominated by fluctuations of the local moments, as in an actual ferromagnet. Therefore, the threshold value of D for the FM-PM transition depends only weakly on N as compared to the UV-FM transition. At some value of N between 160 and 180, the UV phase decays directly to the PM phase, indicating that for $N \gtrsim 180$ and $\beta = 25$ the UV+FM phase coexistence zone extends to the boundary of the PM phase.

3 Supplementary Videos

In all videos the dashed blue lines indicate the critical isocline, while the orange dashed lines in videos 3 and 4 indicate the $1/\beta$ line.

Video 1: Radially Polarized (RP) phase (`Video1-RP.mp4`)

This video captures the dynamic behavior of the radially polarized (RP) phase when a small noise ($D = 0.05$) is added. Other parameters are $\beta = 0.5$, $N = 350$, and $\sigma = 0.1$. The right side displays real-time polar order parameters of the system. The added noise results in a highly fluid behavior, while still retaining a high degree of radial polar order, as corroborated by the high values of P_r.

Video 2: Orbiting Ferromagnetic (FM) phase (`Video2-FM.mp4`)

This video shows the evolution of the FM phase for $(\beta, D, N, \sigma) = (10.0, 1.0, 350, 0.1)$. Despite the considerably high noise, the phase remains qualitatively unchanged with respect to the noiseless case, showcasing its superior noise tolerance compared to other ordered phases.

Video 3: Uniform vortex (UV) phase (`Video3-UV.mp4`)

This video presents two distinct perspectives of the UV phase captured in a single simulation run with parameters $(\beta, D, N, \sigma) = (1.85, 0.0, 500, 0.1)$: (left) laboratory-frame view, with colors representing the orientation angles (θ) of the particles; and (right) rotating-frame view, with colors representing the tilt angles ($\chi = \theta - \phi$) relative to the radial axis. The video highlights the markedly different behavior of polar orientations for particles within regions $r > 1/\beta$ compared to those within $r < 1/\beta$. Our quasi-rigid-body model accurately captures this distinction, as discussed in the main text. The rotating-frame view provides a clearer visualization of collective deformations within the cluster, revealing a subtle wobbling of the inner region relative to the outer region.

Video 4: Shear-banded vortex (SBV) phase (`Video4-SBV.mp4`)

This video illustrates both lab-frame and rotating-frame views of the Shear-banded vortex (SBV) phase in a simulation run with $(\beta, D, N, \sigma) = (1.85, 0.0, 350, 0.1)$. Notably, particles in the inner region rotate on average in the opposite direction to the outer bulk, defining the characteristic emergent shear banding. The rotating frame view enhances the visualization of crucial points discussed in the main text: (i) The reddish shades of particles in the inner region (that is, $\chi \simeq 0$) reveal their tendency to align radially; (ii) Particles in the bulk (outer region) undergo sporadic rearrangements, facilitating the exchange of particles between both regions. These features are essential for understanding the shear-banding transition.

Video 5: Multi-cluster phase (`Video5-Clusters.mp4`)

This video illustrates the evolution of the multi-cluster phase for $(\beta, D, N, \sigma) = (5.0, 0.0, 93, 0.1)$. Here, the system separates into 4 different clusters, each one showcasing traits similar to the FM phase, but orbiting the potential well as a vortex phase. The global vortex-like

behavior is evidenced by the high values of P_ϕ. Note that $|\boldsymbol{P}|$ is close to zero since we are taking all particles into account, and thus the clusters in opposing sides cancel each other. The value of $|\boldsymbol{P}|$ considering only the particles inside a cluster is close to 1.

References

[1] Olivier Dauchot and Vincent Démery Phys. Rev. Lett. 122, 068002 (2019).

[2] Rubens H. Damascena, Leonardo R. E. Cabral, and Clécio C. de Souza Silva, Phys. Rev. E 105, 064608 (2022).

[3] See Eqs. (4.3.133) and (4.3.135) of Milton Abramowitz and Irene A. Stegun, Handbook of Mathematical Functions with Formulas, Graphs, and Mathematical Tables. ninth Dover printing, tenth GPO printing New York: Dover (1964).

[4] I. S. Gradshteyn and I. M. Ryzhik, Table of integrals, series, and products. Seventh edition: Elsevier/Academic Press, Amsterdam (2007).